

RuO₂/TiO₂/Pt Ternary Photocatalysts with Epitaxial Heterojunction and Their Application in CO Oxidation

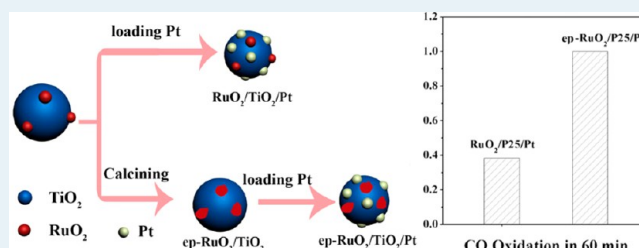
Yanchao Jiao, Hailin Jiang, and Feng Chen*

Key Laboratory for Advanced Materials and Institute of Fine Chemicals, East China University of Science and Technology, 130 Meilong Road, Shanghai 200237, China

Supporting Information

ABSTRACT: Coexisting oxidation and reduction cocatalysts play a significant role in the photocatalytic oxidation reaction. Here a surface modification method was used to synthesize the ternary photocatalyst RuO₂/TiO₂/Pt with RuO₂ nanoclusters of ca. ~2 nm size. Further, thermal treatment was adopted to transform RuO₂ nanoclusters into an epitaxial layer on the surface of TiO₂ to form ep-RuO₂/TiO₂/Pt. XRD, TEM, and XPS were used to verify the formation of the RuO₂ epitaxial layers on both rutile and anatase TiO₂. The interfacial atom arrangement match between the RuO₂ and TiO₂ is suggested as the possible physical basis for the transformation process of RuO₂ from nanoparticles to epitaxial layers. The photocatalytic performance of RuO₂/TiO₂/Pt and ep-RuO₂/TiO₂/Pt was studied by photocatalytically oxidizing gaseous CO under the UV irradiation. The optimal RuO₂ contents in the ep-RuO₂/TiO₂/Pt were 0.05, 0.1, and 0.02 wt % for P25, commercial anatase, and commercial rutile TiO₂, respectively. In their optimal RuO₂ contents, the photocatalytic activity of the ep-RuO₂/TiO₂/Pt for CO oxidation are ca. 2.6, 2.4, 1.7 times than that of their uncalcined ones and ca. 20, 15, 8 times that of their corresponding bare TiO₂ for P25, anatase, and rutile, respectively. The formation of interfacial epitaxial RuO₂ layers leads to more significant exposure of RuO₂ (110) facets in the ep-RuO₂/TiO₂/Pt ternary photocatalyst, which plays an effective role in promoting photocatalytic CO oxidation.

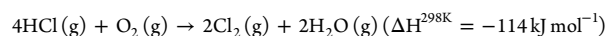
KEYWORDS: ternary photocatalysts, epitaxial heterojunction, CO oxidation, TiO₂, RuO₂



INTRODUCTION

As an inevitable indoor air pollutant,^{1–4} CO pollution has become a public health concern during the past several decades because of the increase in the incidence of respiratory infections, including pneumonia, cardiovascular events, and all-cause mortality in both adults and children.^{1–3} In crowded areas, such as the public schools,⁵ the subway stations,⁶ the restaurants,⁷ as well as the meeting rooms and the garages, the CO concentrations in these indoor air spaces are always beyond the allowable limit (for instance, a limit of 8.73 ppm in 1 h in China,⁸ and 30.56 ppm in 1 h in Europe⁹). So far, various technologies have been investigated to achieve the indoor CO elimination, among which TiO₂ photocatalysis is a very promising candidate.^{10–13} Nano-TiO₂ is an environmentally friendly material and has been widely applied in air and water purifications via photocatalysis.^{2,14–17} As we know, the important photocatalytic redox processes with the photo-generated electrons and holes generally take place on the surface of the catalyst. Hence, in order to achieve better photocatalytic performances, numerous surface modification strategies have been frequently used to the TiO₂ nanomaterials. For instance, the enhanced H₂ production with TiO₂-g-C₃N₄,¹⁸ TiO₂-CuO,¹⁹ TiO₂-MoS₂,²⁰ Pt/TiO₂,²¹ TiO₂-NiO,¹⁵ and the better photocatalytic oxidation performance of TiO₂-CeO₂,²² TiO₂-RuO₂,²³ and TiO₂-IrO₂.²⁴

Accordingly, combining an excellent oxidation catalyst with TiO₂ would be very likely to enhance the photocatalytic oxidation performance of TiO₂. RuO₂ is a very powerful oxidation catalyst and well-known for its applications in the Deacon process^{25–28} in industrial production of Cl₂ by oxidizing the gaseous HCl, which is shown as follows:



The applications of RuO₂ in heterogeneous catalysis are much more beyond the Deacon process. As summarized in a recent review,²⁹ numerous molecules, such as CO, CO₂, H₂O, O₂, NH₃, NO, methanol, ethylene, and methane, adsorb well on the RuO₂(110) surface via the under-coordinated Ru atoms, which is a prerequisite for catalytic reactions.

A recent work indicated that rutile TiO₂ and RuO₂ share the same type of lattice symmetry and have almost the same lattice parameters (particularly, $a = 4.59 \text{ \AA}$, $c = 2.96 \text{ \AA}$ for rutile and $a = 4.49 \text{ \AA}$, $c = 3.10 \text{ \AA}$ for RuO₂).³⁰ When the compound of RuO₂ (with size ~sub 2 nm) and rutile TiO₂ is thermally treated, the RuO₂ grows along the TiO₂ surface, and finally forms a unique heterostructure at the interface, which is composed of RuO₂ epitaxial layer and TiO₂ grain. Applying

Received: January 24, 2014

Revised: May 14, 2014

Published: June 2, 2014

RuO₂/TiO₂ composites in the Deacon Process showed that the spread of RuO₂ on the TiO₂ promotes significantly its oxidation catalytic performance.^{30,31} Further, an experimental tracking of catalytic activity of RuO₂/TiO₂ over time suggests the epitaxial layer of RuO₂ on TiO₂ is quite chemically stable and well-kept in STEM observation throughout the catalytic process.³⁰

Meanwhile, noble metal clusters (Pt, Ag, Au) are frequently used to improve the photocatalytic performances of TiO₂.^{11–13,32–35} Besides the Schottky barrier effect, which significantly promotes the electron/hole separation in TiO₂ photocatalysis, noble metal clusters themselves are quite good redox catalyst.^{10,12,36} For instance, Hwang et al.¹³ verified that Pt nanoparticles at the surface of TiO₂ provide surface sites to stabilize the active oxygen species, thus enhancing the CO photooxidation. Early in 1980s, Gratzel et al.^{37–41} reported that coloading of Pt and RuO₂ onto TiO₂ (or CdS) greatly increases the quantum yield of the H₂ and O₂ generation in the photocatalytic H₂O cleavage, whereas a very recent survey by Li et al.⁴² shows that coloading of Pt and RuO₂ nanoclusters onto TiO₂ photocatalyst leads to a significantly improved photocatalytic activity for the oxidation of sulfur-containing organic compounds. RuO₂ promotes the transfer of the photogenerated holes to the surface of the photocatalysts and facilitates the surface oxidation reaction of holes, whereas Pt is helpful to the transferring and reaction of the electrons.^{37–42}

Although the RuO₂/TiO₂ composites have been investigated in photocatalysis,^{33,42,43} the role of RuO₂ epitaxial spreading on TiO₂ grains in the photocatalysis has not yet been analyzed. Aiming at this issue, RuO₂/TiO₂/Pt ternary photocatalysts were synthesized in this work, and their reactivity to the photocatalytic oxidation of gaseous CO before and after the epitaxial spreading of RuO₂ was observed. Particularly, the epitaxial growth property of RuO₂ over different crystal phases of TiO₂ (anatase, rutile, and their mixture) was carefully investigated. Interestingly, the epitaxial growth of RuO₂ on the surface of anatase was also verified in this work, which, to our knowledge, has not been reported yet.

Briefly, RuO₂/TiO₂/Pt ternary composites (photocatalyst: TiO₂, dual cocatalyst: RuO₂ and Pt) were prepared with a surface modification method, in which RuO₂ can transform into an epitaxial layer on the surface of TiO₂ under thermal treatment. The epitaxial growth property of RuO₂ on the various TiO₂ supports, as well as its role on photocatalytic oxidation of CO, was investigated in this work.

EXPERIMENTAL SECTION

Materials Synthesis. *Synthesis of RuO₂-Loaded TiO₂ (RuO₂/TiO₂).* P25 TiO₂ (Evonik Degussa), anatase (A-60, Dacheng Nanotech Co.), and rutile (R-100, Dacheng Nanotech Co.) were all from commercial sources. A hydrothermal method was used to prepare RuO₂/TiO₂ catalysts just as previously reported.³⁰ A desired amount of RuCl₃ was mixed with the specified TiO₂ (P25, anatase, and rutile) in different ratios using water as the solvent. Then the mixture was transferred into a 100 mL autoclave and heated at 180 °C for 10 h. The as-formed powders were separated by centrifugation, washed several times with deionized water, and dried at 60 °C under vacuum overnight to obtain the RuO₂/TiO₂ catalysts.

To obtain an epitaxial layered structure for RuO₂, RuO₂/TiO₂ composites were further calcined under 400 °C for 10 h in air, which was denoted as ep-RuO₂/TiO₂.

Synthesis of RuO₂/TiO₂/Pt and ep-RuO₂/TiO₂/Pt. RuO₂/TiO₂/Pt photocatalysts were prepared by a photoreduction

method. Typically, 0.1 g of RuO₂/TiO₂ nanocomposite was mixed with 7.9 mL of H₂PtCl₆ solution (1.0 g/L) followed by the addition of 100 mL of methanol/H₂O solution (25% v/v methanol/H₂O). The suspension was magnetically stirred for 3 h under UV (300 W high pressure Hg lamp) illumination. After irradiation, the samples were centrifuged, washed, and then dried at 60 °C under vacuum overnight to obtain RuO₂/TiO₂/Pt (nominal Pt content 3.0 wt %). Ep-RuO₂/TiO₂/Pt catalysts were prepared with the same procedure except that ep-RuO₂/TiO₂ was used instead of RuO₂/TiO₂.

Materials Characterization. The crystalline phase of products was examined by powder X-ray diffraction (XRD). Diffraction patterns of the samples were performed using an X-ray diffractometer (Rigaku Ultima IV) operating in the reflection mode with Cu K α radiation at a scan rate of 0.02° 2 s⁻¹. Transmission electron microscopy (TEM) was performed using a JEOL JEM 2100F instrument operated at 200 kV. To prepare the TEM specimens, the powder samples were first dispersed ultrasonically in anhydrous ethanol in a centrifuge tube for nearly 10 min. After allowing the centrifuge tube to stand for 5–10 min, one drop of the supernatant suspension was dropped onto a carbon-film-supported copper grid and allowed to dry in air before the specimens were transferred into the microscope. The instrument employed for XPS studies was a Thermo Fisher ESCALAB 250Xi system with Al K α radiation (photon energy of 1361 eV) and calibrated internally by carbon deposit C (1s) binding energy (BE) at 284.6 eV.

Photocatalytic Reaction. The photocatalytic oxidation processes were carried out in a closed loop gas-flow system at ambient temperature and pressure. The photocatalytic reactor was made of a horizontal quartz tube with a flange connection. A quartz plate loaded the assigned catalyst (5.0 cm × 11.0 cm) was laid across the tube for photocatalytic use. The reactor was connected to a circulation pump through an external Teflon tubing (o.d. 0.32 cm) to push the gas in the system in the dynamic loop. The gas circulation flow rate was about 2 L·min⁻¹. A 300 W high pressure mercury lamp (Shanghai Yaming Lighting Co., Ltd.) was horizontally fixed 20 cm above the photocatalytic reactor, and the light intensity illuminated on the catalyst was ca. 1.0 mW·cm⁻². The CO concentration variation during the reaction was determined real-time by an online CO detector (KB-501X, Kesa Electronics Co., Ltd.) with a CO analytic sensitivity of 1 ppmv. The closed system was prefilled by pure dry air (99.9995%), and then a desired amount of CO was injected into the system to reach a concentration of 470 ppmv. When the CO molecules in the system reached equilibrium, we then initiated the photocatalytic reaction by removing the optical mask between the reactor and the UV lamp.

RESULTS AND DISCUSSION

Characterization of the Photocatalyst. To reveal the relationship of the epitaxial growth property of RuO₂ with the TiO₂ lattice, three kinds of TiO₂, that is, P25 (mixture of anatase and rutile, S_{BET} = 65 m²/g), anatase (S_{BET} = 64.7 m²/g), and rutile (S_{BET} = 105.9 m²/g) (see Table S1), were adopted to track the morphology evolution of RuO₂ nanoclusters on them.

XRD patterns of TiO₂ before and after the RuO₂ deposition (Figure 1 and Figures S1–S3) only exhibit the typical TiO₂ XRD signals. No characteristic peak for RuO₂ can be observed for all three kinds of RuO₂/TiO₂ composites. The FWHMs of the XRD signals for TiO₂ have no change after loading the

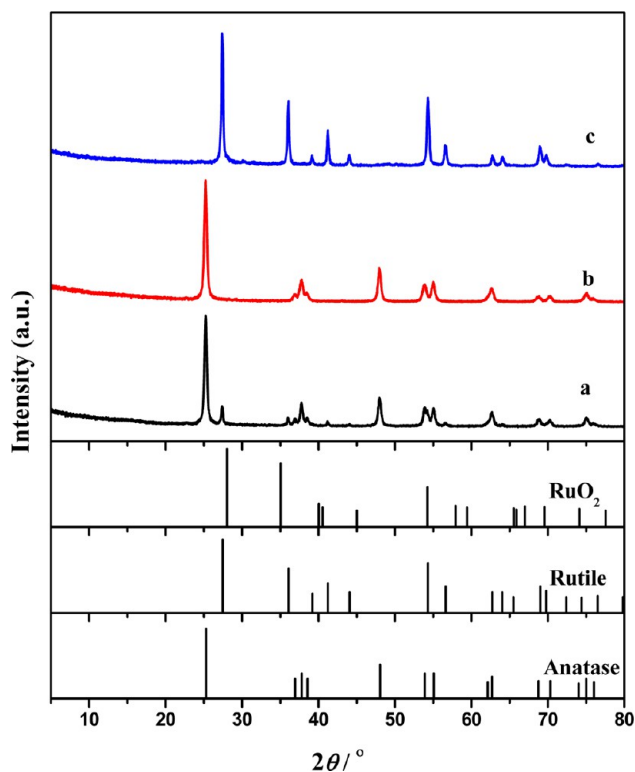


Figure 1. XRD patterns of (a) 0.2% RuO₂/P25, (b) 0.2% RuO₂/anatase, and (c) 0.2% RuO₂/rutile.

RuO₂ compound, which indicates that the grain size of TiO₂ does not change obviously.

Figure 2 shows the TEM images of various RuO₂/TiO₂ and RuO₂/TiO₂/Pt materials. The TEM image of RuO₂/P25 (Figure 2A₁) shows some small nanoclusters (~2 nm, Figure S7 for detailed size distribution) on the surface of the relatively bigger ones (~25 nm). The bigger ones are the P25 TiO₂ nanoparticles, and the smaller ones should be ascribed to RuO₂ nanoclusters. It is confirmed that RuO₂ species of ~2.0 nm in size can be smoothly synthesized under hydrothermal treatment of 180 °C.³⁰ One should note that a small size of RuO₂ clusters has been suggested to be crucial for the formation of epitaxial layers on TiO₂.³⁰ Similar results are also observed for RuO₂/anatase (Figure 2B₁) and RuO₂/rutile (Figure 2C₁) composites, of which RuO₂ nanoclusters were deposited as small as ~2 nm. After calcinations, the RuO₂ nanoclusters disappear (Figure 2A₂, B₂, and C₂), which should be ascribed to the RuO₂ epitaxial spreading and should not be confused with the solid dissolution. It has been observed in the literature that the very small RuO₂ nanoparticles can epitaxially grow along with the surface of TiO₂ under calcinations,³⁰ as their lattice parameters (particularly, $a = 4.59 \text{ \AA}$, $c = 2.96 \text{ \AA}$ for rutile and $a = 4.49 \text{ \AA}$, $c = 3.10 \text{ \AA}$ for anatase) are almost the same.³¹ Formation of the epitaxial layers can be further verified with the subsequent XPS observation. One may note that the epitaxial growth of RuO₂ also occurred on the surface of anatase, which, to our knowledge, has not yet been mentioned in the literature. The TEM observation of RuO₂/TiO₂ in Figure 2 reveals that the epitaxial structure of RuO₂ can form well on different crystals of TiO₂.

After the photoreduction, some small grains with darker color (~3 nm, Figure S8 for detailed size distribution) formed on the surface of TiO₂ as shown in Figure 2A₃, B₃, and C₃.

According to its interplanar space of 0.23 nm (a characteristic lattice fringe of (111) of Pt crystals), the new-formed darker grains with a size of ca. 3 nm can be deduced as Pt nanoclusters. Further, the Pt nanoclusters can also smoothly formed on the ep-RuO₂/TiO₂ as shown in Figure 2A₄, B₄, and C₄, in which only Pt nanoclusters but no RuO₂ clusters can be observed.

The chemical properties of the as-prepared composites were further characterized with the XPS technique (Figure 3). The XPS signals of Ti do not have any obvious change throughout the work (as shown in Figure S4). The peak of the Ru element can be obviously observed from the positions of the Ru 3d_{5/2} line around 280.6 eV. The XPS signals with binding energies larger than 283.0 eV are due to the C element from the C adhesive. Before the calcinations, the Ru element has two XPS signals centered at 280.6 and 282 eV. After the calcinations, it is obvious that the signals at 282 eV are significantly reduced, as shown in the right half of Figure 3; meanwhile, after high-temperature treatment, the signals at 280.6 eV shift slightly to about 280.3 eV, which can be attributed to 1f-cus (stands for one fold under-coordinated Ru atoms) Ru atoms on the RuO₂ (110) surface based on DFT calculations.⁴⁴ It is known that epitaxial spread of RuO₂ on the TiO₂ substrate results in a greater amount of 1f-cus Ru atoms at the enlarged RuO₂ surface. Generally, the XPS signals at 280.3 eV correspond to surface Ru atoms, whereas those at 282 eV correspond to bulk Ru atoms in RuO₂.²⁹ Considering that the nano-grain morphology of RuO₂ cannot be captured in the TEM images (Figure 2A₂, B₂, and C₂) after calcinations, the existing form of RuO₂ here should be changed. It has been known that the distorted RuO₆ octahedron of RuO₂ consists of two non-equivalent groups of O atoms: four equatorial O atoms forming Ru–O bonds of 1.98 Å and two apical O atoms having a Ru–O bond length of 1.94 Å.^{29,45} That is quite near to the Ti–O distances of 1.98 and 1.93 Å in the TiO₆ octahedron of anatase and 1.98 and 1.95 Å of rutile.^{46,47} Considering the interesting changes in the TEM and XPS observations, the RuO₂ grains here should epitaxially grow along with the surface of anatase, which make them disappear from the TEM observation. Consequently, the unique layered heterojunction structure is successfully formed for RuO₂ at the interface of the three kinds of TiO₂ materials. Briefly, RuO₂/TiO₂/Pt ternary composites (photocatalyst: TiO₂, dual cocatalyst: RuO₂ and Pt) were prepared with all three kinds of TiO₂ (P25/anatase/rutile), of which RuO₂ forms epitaxial layers on the surface of TiO₂ under thermal treatment.

Mechanism Explanation for Epitaxial Spreading of RuO₂ on TiO₂. As shown in Scheme 1, the (101) plane is a typical exposed facet for anatase TiO₂. Anatase TiO₂ is composed of [TiO₆] octahedra, and the Ti–O bonds at (101) plane have lengths of 1.98 and 1.93 Å (Scheme 1); meanwhile, RuO₂ consists of [RuO₆] octahedra with Ru–O bonds of 1.98 and 1.94 Å. Therefore, when RuO₂ is epitaxial spreading along the (101) plane of anatase, only a very slight stress would occur from the atom arrangement mismatch between the RuO₂ and anatase. In a word, the good degree of inherent lattice match (Scheme 1) between RuO₂ and anatase TiO₂ contributes the physically basic factor for the epitaxial growth of RuO₂ on anatase TiO₂. By analogy, an M–O bond match between the RuO₂ and rutile TiO₂ should also be possible, favoring the epitaxial spreading of RuO₂ on rutile.^{30,31}

Academically, because RuO₂ is a more active oxidation catalyst than TiO₂, a larger exposed surface area of RuO₂ to the CO would greatly benefit the surface oxidation reaction of CO

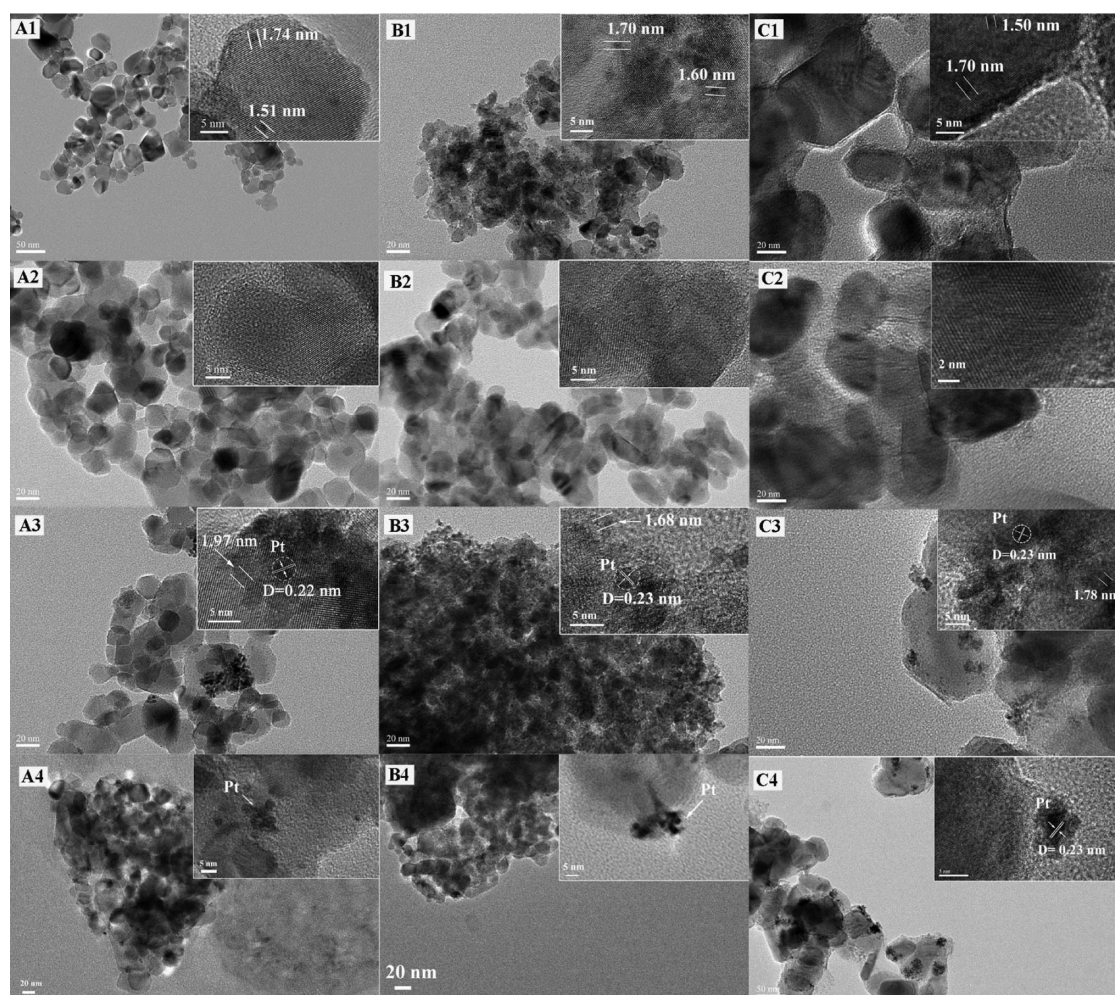


Figure 2. TEM images of typical (A1) RuO₂/P25, (A2) ep-RuO₂/P25, (A3) RuO₂/P25/Pt, (A4) ep-RuO₂/P25/Pt; (B1) RuO₂/anatase, (B2) ep-RuO₂/anatase, (B3) RuO₂/anatase/Pt, (B4) ep-RuO₂/anatase/Pt; (C1) RuO₂/rutile, (C2) ep-RuO₂/rutile, (C3) RuO₂/rutile/Pt, and (C4) ep-RuO₂/rutile/Pt. Insets: corresponding magnified images.

with O₂. The epitaxial layers transformation process of RuO₂ on TiO₂ is illustrated in Scheme 2. The formation process involves two steps: (1) RuO₂ nanoclusters with size of ca. ~2 nm on TiO₂ were hydrothermally synthesized and (2) RuO₂ nanoparticles transform into epitaxial layers on the surface of TiO₂ under calcination. The calcination is the decisive step for the formation of the epitaxial structure. Consequently, a unique layered heterojunction structure at the interface of RuO₂/TiO₂ on all TiO₂ materials.

Photocatalytic Performance of Hybrid Catalysts.

Generally, noble-metal-loaded TiO₂ is considered as a potential candidate for CO oxidation. Hence, the CO oxidation with P25, P25/Pt, 0.05%RuO₂/P25/Pt, and ep-0.05%RuO₂/P25/Pt catalysts were checked in the dark (Figure 5S), which shows very slow concentration decreases of CO in all cases. Figure 4 shows the photocatalytic oxidation of CO on P25, P25/Pt, and RuO₂/P25/Pt. Bare P25 exhibits relatively low activity for photocatalytic oxidation of CO (30.8% in 6 h), and the activity is enhanced significantly by loading Pt nanoclusters (69.7% CO oxidation in 6 h). As an effective oxidation catalyst, co-loading of RuO₂ (0.05 wt %) with Pt nanoclusters on P25 TiO₂ further promotes the photocatalytic activity of the catalyst, which oxidatively converts 100% CO within 3 h. Most interestingly, although Pt-free 0.05%RuO₂/P25 and ep-0.05%RuO₂/P25

catalysts shows similar photocatalytic activity as that of P25, ternary photocatalyst with an epitaxially spread RuO₂ heterojunction, that is ep-RuO₂/P25/Pt, exhibits the maximum photocatalytic activity in CO oxidation. The conversion of CO reaches 100% within just 1 h in this case, much higher than those with other catalysts, such as P25 or P25/Pt and even the uncalcined RuO₂/P25/Pt catalyst. The CO concentration decrease in Figure 4 can be fit well with zero-order kinetics, of which the apparent reaction rate constants of CO oxidation are $0.85 \times 10^{-3} \text{ min}^{-1}$, $1.9 \times 10^{-3} \text{ min}^{-1}$, $6.3 \times 10^{-3} \text{ min}^{-1}$, and $16.7 \times 10^{-3} \text{ min}^{-1}$ with P25, P25/Pt, RuO₂/P25/Pt, and ep-RuO₂/P25/Pt, respectively. In a word, the photocatalytic activity of the ternary photocatalyst increases by nearly 7 times of bare P25 and is ca. 20-fold that of P25 due to the epitaxial growth of RuO₂ on the surface of TiO₂. It can be speculated that coloaded Pt and RuO₂ have a synergistic effect in improving the photocatalytic performance of P25 TiO₂ in the CO oxidation. This may be attributed to the suitable energy band matching between the cocatalysts and semiconductor. Loaded RuO₂ traps the photoholes, whereas loaded Pt traps the photoelectrons, so that such a surface modification favors most the separation of photoinduced electrons and holes and dramatically improves the photocatalytic efficiency of the photocatalyst.

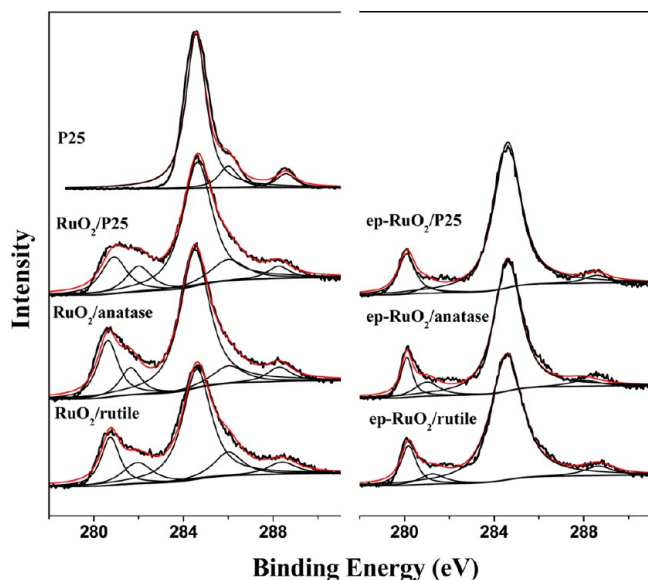
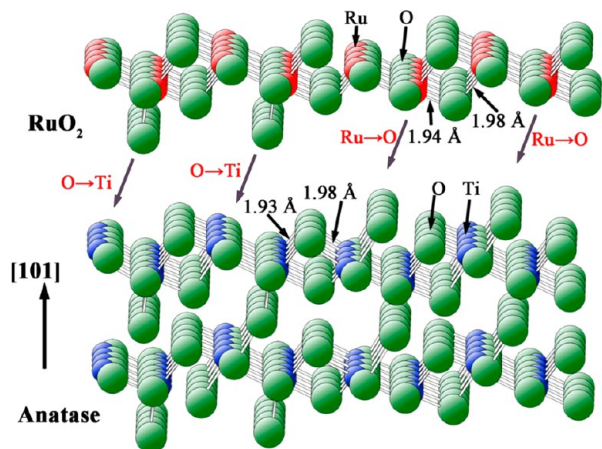


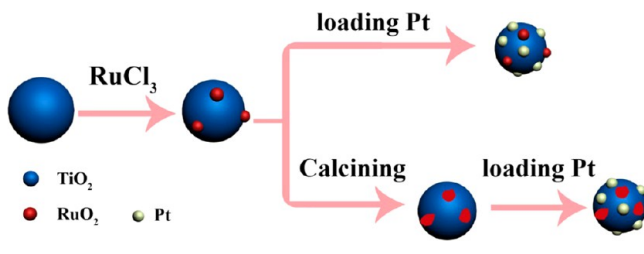
Figure 3. XPS fine spectra of Ru $3d_{5/2}$ region of P25 (TiO_2), $\text{RuO}_2/\text{P25}$, $\text{RuO}_2/\text{anatase}$, $\text{RuO}_2/\text{rutile}$ (left half of the figure), and ep- $\text{RuO}_2/\text{P25}$, ep- $\text{RuO}_2/\text{anatase}$, ep- $\text{RuO}_2/\text{rutile}$ (right half of the figure). * 280.4 ± 0.2 eV is the surface Ru atoms signal, 281.8 ± 0.2 eV is the bulk Ru atoms signal, and binding energy >283.0 eV is ascribed to the C 1s signals.

Scheme 1. Atom Arrangement at (101) Lattice Plane of Anatase and Corresponding Atom Arrangement of RuO_2 at Their Interface^a



^aBlue balls are the Ti atoms, the green balls are the O atoms, and the red balls mean the Ru atoms.

Scheme 2. Schematic Illustration of the Formation of Epitaxial Layers of RuO_2 on TiO_2 Support



The photocatalytic activity of the ternary photocatalysts should be closely related to the loading amount of RuO_2 .

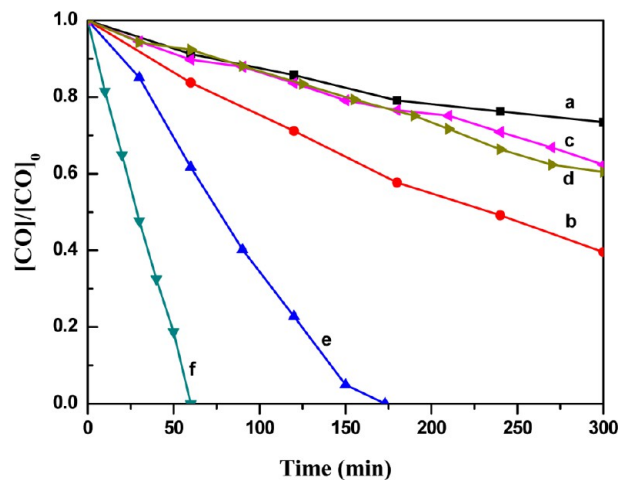


Figure 4. Photocatalytic oxidation of CO with (a) P25, (b) P25/Pt, (c) 0.05% $\text{RuO}_2/\text{P25}$, (d) ep-0.05% $\text{RuO}_2/\text{P25}$, (e) 0.05% $\text{RuO}_2/\text{P25}/\text{Pt}$, (f) ep-0.05% $\text{RuO}_2/\text{P25}/\text{Pt}$ catalysts.

Therefore, the photocatalytic oxidation of CO was also observed with the ternary photocatalyst versus the loading amount of RuO_2 (0–0.2 wt %), either before (RuO_2 in nanoclusters, Figure 5) or after the calcination (epitaxial

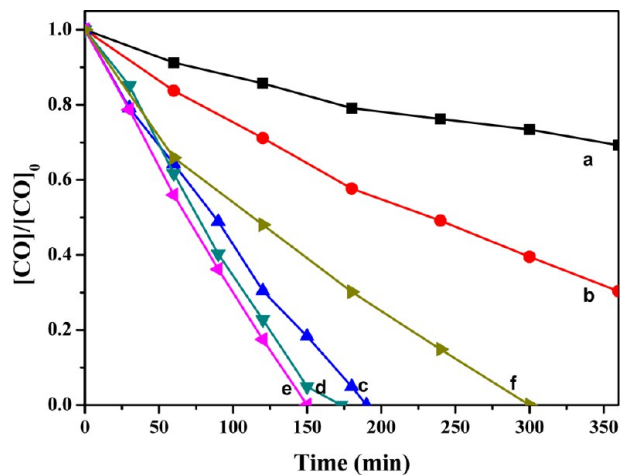


Figure 5. Photocatalytic oxidation of CO with (a) P25, (b) P25/Pt, (c) 0.02% $\text{RuO}_2/\text{P25}/\text{Pt}$, (d) 0.05% $\text{RuO}_2/\text{P25}/\text{Pt}$, (e) 0.1% $\text{RuO}_2/\text{P25}/\text{Pt}$, (f) 0.2% $\text{RuO}_2/\text{P25}/\text{Pt}$.

spreading of RuO_2 , Figure 6). Bare P25 and P25/Pt photocatalyst convert about 30.8% and 69.7% of the CO in 300 min, respectively. Both are not favorable for the CO photocatalytic oxidation application as shown in Figure 5. Before calcination, the reactivity of the ternary photocatalyst initially increases with the increase amount of loaded RuO_2 , and it reaches the maximum at RuO_2 loading amount of 0.1 wt %. A CO content of 470 ppm can be totally converted within 150 min. Further increasing the amount of RuO_2 leads to a decrease in the photocatalytic activity. As shown in Figure 5, the oxidation of CO with the 0.2% $\text{RuO}_2/\text{P25}/\text{Pt}$ is however slower than that with the 0.1% $\text{RuO}_2/\text{P25}/\text{Pt}$ and is completely achieved until after 300 min UV irradiation.

Calcination is the decisive step in the epitaxial structure formation of the ternary photocatalyst. As shown in Figure 6, the photocatalytic oxidation of CO with the ternary photocatalysts is highly increased after the calcinations. The

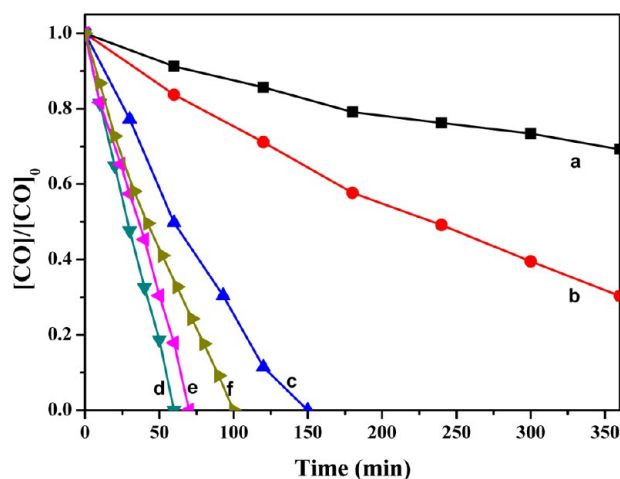


Figure 6. Photocatalytic oxidation of CO with (a) P25, (b) P25/Pt, (c) ep-0.02%RuO₂/P25/Pt, (d) ep-0.05%RuO₂/P25/Pt, (e) ep-0.1%RuO₂/P25/Pt, (f) ep-0.2%RuO₂/P25/Pt.

photocatalytic apparent reaction rate constants of CO oxidation with the ternary photocatalysts with 0.02, 0.05, 0.1, and 0.2 wt % RuO₂ show a 1.3, 2.9, 2.1, and 3.0 times increase along with the epitaxial structure formation for the ternary photocatalysts, respectively. The ep-0.05% RuO₂/P25/Pt ternary photocatalyst (0.05 wt % RuO₂) exhibits the highest photocatalytic activity, as shown in Figure 6.

The RuO₂ nanoclusters on the TiO₂ catalyst play an important role due to its excellent oxidation performance in the redox reaction. The epitaxial spreading of RuO₂ on the P25 TiO₂ increases the apparent reaction rate constant of CO oxidation as large as ca. 3 times, as shown in Figures 5 and 6. Although more surface of TiO₂ was covered with RuO₂ after its epitaxial spreading, the formation of RuO₂ epitaxial layers exposes more facets of RuO₂, which as a whole exhibits a positive effect for the CO photocatalytic oxidation.

Figure 7 shows the photocatalytic oxidation of CO with anatase, anatase/Pt, RuO₂/anatase/Pt, as well as ep-RuO₂/

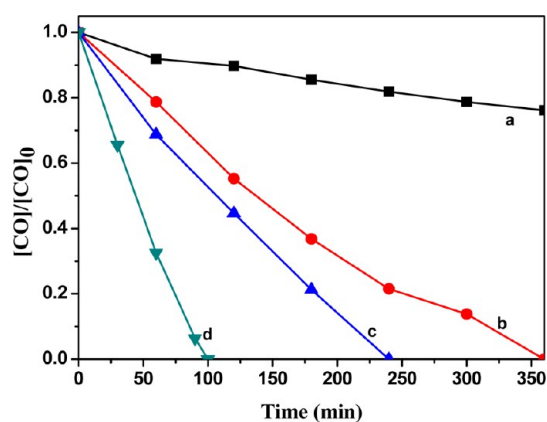


Figure 7. Photocatalytic oxidation of CO with (a) anatase, (b) anatase/Pt, (c) 0.1%RuO₂/anatase/Pt, (d) ep-0.1%RuO₂/anatase/Pt.

anatase/Pt. A similar trend can be observed as that with P25 series photocatalysts. Bare anatase exhibits low activity for the photocatalytic oxidation conversion of CO, which gives 23.8% in 6 h. The oxidation of CO is enhanced by loading Pt nanoclusters onto the anatase, which reaches to 100% in 6 h. Due to the good performance of RuO₂ in the catalytic oxidation

process, coloaded of RuO₂ nanoclusters with Pt further improves the activity of the photocatalysts, with which 100% conversion of CO is achieved within just 4 h. Epitaxial spreading of RuO₂ via the calcination on the anatase TiO₂ significantly promotes the beneficial role of RuO₂ cocatalyst in the ternary photocatalyst (ep-RuO₂/anatase/Pt). A complete conversion of CO was rapidly achieved in just 100 min with the ep-RuO₂/anatase/Pt, as shown in Figure 7. The apparent reaction rate constants of CO oxidation are $0.66 \times 10^{-3} \text{ min}^{-1}$, $4.2 \times 10^{-3} \text{ min}^{-1}$, and $10.0 \times 10^{-3} \text{ min}^{-1}$ with anatase, RuO₂/anatase/Pt, and ep-RuO₂/anatase/Pt, respectively. Notably, the photocatalytic activity of the ternary photocatalyst increases more than 6 times of bare anatase and is 15 times that of anatase due to the epitaxial growth of RuO₂ on the surface of TiO₂.

The photocatalytic oxidation of CO with RuO₂/anatase/Pt series ternary photocatalysts before (Figure 8) and after (Figure

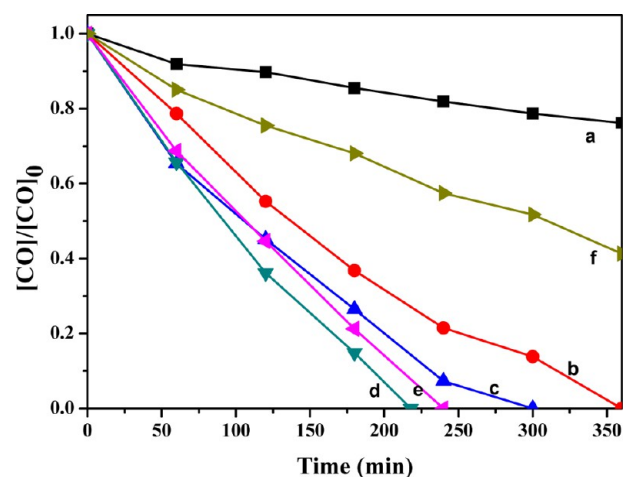


Figure 8. Photocatalytic oxidation of CO with (a) anatase, (b) anatase/Pt, (c) 0.02%RuO₂/anatase/Pt, (d) 0.05%RuO₂/anatase/Pt, (e) 0.1%RuO₂/anatase/Pt, (f) 0.2%RuO₂/anatase/Pt.

9) the calcination was also investigated. Obviously, RuO₂ loading leads to an increase in photocatalytic activity for the anatase photocatalysts. Specifically, 0.05% RuO₂/anatase/Pt

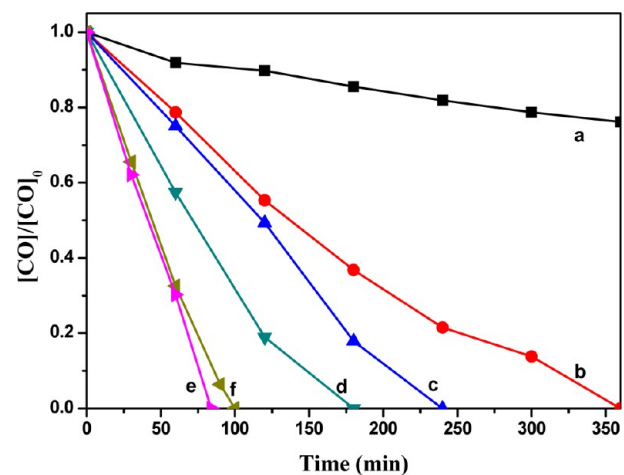


Figure 9. Photocatalytic oxidation of CO with (a) anatase, (b) anatase/Pt, (c) ep-0.02%RuO₂/anatase/Pt, (d) ep-0.05%RuO₂/anatase/Pt, (e) ep-0.1%RuO₂/anatase/Pt, (f) ep-0.2%RuO₂/anatase/Pt.

and 0.1% RuO₂/anatase/Pt show higher activities than the others, with which CO was totally converted within 210 and 240 min, respectively. By comparison with Figure 8, the ternary photocatalysts which have epitaxial heterogeneous structure (ep-RuO₂/anatase/Pt) show highly enhanced photocatalytic activities as shown in Figure 9. Particularly, the ep-RuO₂/anatase/Pt with 0.1 wt % RuO₂ convert 100% CO within just 100 min, whereas the corresponding uncalcined one (0.1% RuO₂/anatase/Pt) only oxidizes 55.3% CO in 2 h (Figure 8).

With respect to the RuO₂/rutile/Pt ternary photocatalysts, the photocatalytic activities for the CO oxidation (Figures 10

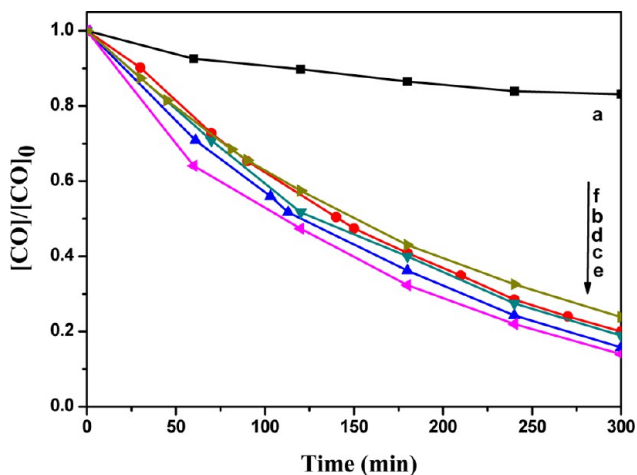


Figure 10. Photocatalytic oxidation of CO with (a) rutile, (b) rutile/Pt, (c) 0.02% RuO₂/rutile/Pt, (d) 0.05% RuO₂/rutile/Pt, (e) 0.1% RuO₂/rutile/Pt, (f) 0.2% RuO₂/rutile/Pt.

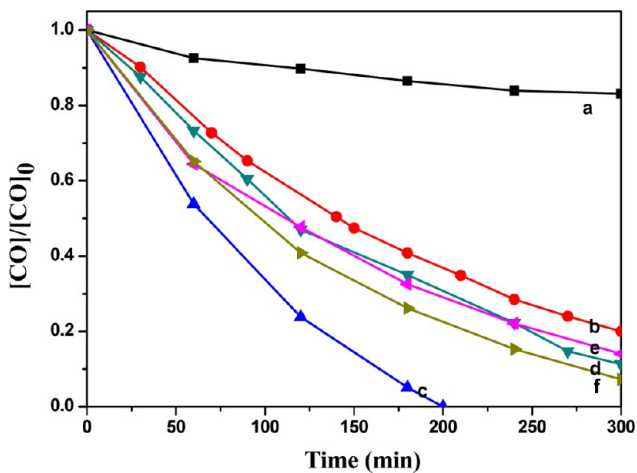


Figure 11. Photocatalytic oxidation of CO with (a) rutile, (b) rutile/Pt, (c) ep-0.02% RuO₂/rutile/Pt, (d) ep-0.05% RuO₂/rutile/Pt, (e) ep-0.1% RuO₂/rutile/Pt, (f) ep-0.2% RuO₂/rutile/Pt.

and 11) are not as good as the former two series. Little in the photocatalytic activity was observed with the RuO₂ loading before the calcinations, as shown in Figure 10. The advantages of RuO₂ for oxidation reaction are not demonstrated after the RuO₂ loading. One possible reason may be due to the difference in redox characters for the exposed lattice facets in rutile TiO₂ compared with those in anatase and P25 TiO₂.^{48–50} RuO₂ nanoclusters here are randomly deposited on the surface

of TiO₂. When the RuO₂ clusters were deposited on the different facets, the effect of RuO₂ deposition can be totally different. Nevertheless, after the calcinations, a promotion to the photocatalytic oxidation of CO begins to appear, as shown in Figure 11. Ep-0.02% RuO₂/rutile/Pt of the highest photocatalytic activity oxidizes all CO in 200 min, whereas the other ep-RuO₂/rutile/Pt photocatalysts also show slightly enhanced photocatalytic activity. Compared with the former two series, the optimal RuO₂ loading amount is only 0.02 wt % for the rutile TiO₂, which should be due to the reactivity differences of the exposed lattice facets for rutile. The ternary photocatalyst has increased the photocatalytic oxidation ability of CO 5 times that of rutile (bare TiO₂), with a further increase to 8 times after the epitaxial spread of RuO₂ nanoparticles on the TiO₂ substrate.

Proposed Mechanism of the Reaction Activity Enhancement with the Epitaxial Heterogeneous Structure. According to the original expectation of our experiment, calcination is the process to obtain the stable epitaxial heterogeneous structures between RuO₂ and TiO₂; as a result, the activity may be increased because of the special exposure of RuO₂ oxidation facets. The reaction activity enhancement by the epitaxial heterogeneous structure can be interpreted as in the following sections. According to the DFT calculations, Seitsonen^{51,52} had reported that the surface energies of bulk-truncated RuO₂ (110), (100), and (101) are 71, 87, and 76 meV/Å², respectively. Generally, the (110) orientation is expected to be the most abundant orientation of polycrystalline RuO₂, where CO molecules adsorb strongly (adsorption energy exceeds 120 kJ/mol) on the 1f-cus Ru atoms. The actual CO oxidation reaction then takes place via recombination with under-coordinated surface oxygen atoms (either bridging O or on-top O atoms).^{51–53} As a main active surface, the exposed area of the (110) facets of RuO₂ in the ternary photocatalyst should be very crucial in determining its photocatalytic oxidation activity.

As the main photocatalyst, TiO₂ absorbs the photons and produces photoelectrons and photoholes. With the addition of Pt and RuO₂ nanoclusters, it is proposed that photoelectrons would transfer to Pt clusters, whereas photoholes transfer to the RuO₂ clusters; therefore, the separation of photoelectrons and photoholes is promoted, and the photocatalytic efficiency of the ternary photocatalyst is greatly enhanced, as shown in this work. However, due to the limitation from the exposed RuO₂ active surface area, the promotion to the surface reaction is limited. Moreover, overloading of RuO₂ is adverse to the photocatalytic activity of ternary photocatalyst, which is probably due to the overoccupying of surface active sites of TiO₂ with RuO₂, which leads to an undesirable increase in the charge recombination.

Fortunately, by constructing interfacial epitaxial layers, the RuO₂ (110) spreads out on the surface of TiO₂ (110), leading to a significant increment of the (110) facets of RuO₂, which play an effective role in CO oxidation. Therefore, as we observed in this work, the photocatalytic performance of the ternary photocatalyst is further enhanced after calcinations. On the other hand, a greater surface of TiO₂ is now covered with the RuO₂ epitaxial layers, which changes the balanced optimal condition for the loading amount of RuO₂ on TiO₂. Differing from those for the uncalcined ternary photocatalyst, the ternary photocatalysts with epitaxially spread RuO₂ reach their optimal RuO₂ content at 0.05, 0.1, and 0.02 wt % for ep-RuO₂/P25/Pt, ep-RuO₂/anatase/Pt, and ep-RuO₂/rutile/Pt, respectively.

CONCLUSION

A surface modification method was used to synthesize the RuO₂/TiO₂/Pt ternary photocatalyst. Three kinds of TiO₂ supports—P25, commercial anatase, and commercial rutile—were used to investigate the epitaxial growth of RuO₂ nanoclusters on the different TiO₂ lattices. RuO₂ nanoclusters smoothly form epitaxial layers on the surface of TiO₂ under calcinations, which exposes more RuO₂ (110) facets in the ternary photocatalysts. A good match of the atom arrangement between the RuO₂ and anatase is suggested as the physical basis for the epitaxial spreading of RuO₂ on the TiO₂. The epitaxial layer structure of RuO₂ on TiO₂ resulted in the formation of a unique layered heterojunction on the interface, which exhibits a significant promotion to the photocatalytic oxidation of CO, much more effective than that with RuO₂ nanoclusters. Under the UV irradiation, the RuO₂ and Pt clusters trap the photogenerated holes and electrons, respectively, and thus synergistically promote the photocatalytic oxidation of CO. The ternary photocatalysts with epitaxial heterogeneous structure show the highest photocatalytic activity for CO oxidation, which are ca. 2.6, 2.4, 1.7 times that of their uncalcined ones and ca. 20, 15, 8 times that of their corresponding bare TiO₂ for P25, anatase, and rutile, respectively.

ASSOCIATED CONTENT

Supporting Information

Details of BET specific surface area (S_{BET}) and average particle size (D) of TiO₂ materials, XRD patterns and DRS spectra of TiO₂ and RuO₂/TiO₂ composites, particle size distributions of RuO₂ and Pt nanoclusters, XPS fine spectra of Ti 2p region, control reactions of CO oxidation in dark, and the apparent reaction rate constant data. This material is available free of charge via the Internet at <http://pubs.acs.org>.

AUTHOR INFORMATION

Corresponding Author

*E-mail: fengchen@ecust.edu.cn. Tel.: +86-21-6425 3056.

Notes

The authors declare no competing financial interest.

ACKNOWLEDGMENTS

This work was supported by the National Nature Science Foundations of China (21177039) and the Innovation Program of Shanghai Municipal Education Commission (13ZZ042).

REFERENCES

- (1) Zhang, J. J.; Smith, K. R. *Environ. Health Perspect.* **2007**, *115*, 848–855.
- (2) Bruce, N.; Perez-Padilla, R.; Albalak, R. *Bull. W. H. O.* **2000**, *78*, 1078–1092.
- (3) Fullerton, D. G.; Bruce, N.; Gordon, S. B. *Trans. R. Soc. Trop. Med. Hyg.* **2008**, *102*, 843–851.
- (4) Smith, K. R.; McCracken, J. P. *J. Exposure Sci. Environ. Epidemiol.* **2010**, *20*, 406–416.
- (5) Chaloulakou, A.; Mavroidis, I. *Atmos. Environ.* **2002**, *36*, 1769–1781.
- (6) Kim, Y. S.; Kim, M. J.; Lim, J. J. *Hazard. Mater.* **2010**, *183*, 448–459.
- (7) Lee, S. C.; Li, W. M.; Chan, L. Y. *Sci. Total Environ.* **2001**, *279*, 181–193.
- (8) *Indoor Air Quality Standards*. National Standard of the People's Republic of China, Report No. GB/T 18883-2003, 2002.

- (9) *World Health Statistics*. Theakston, F.; Mills, B.; Lund, S. World Health Organization: Geneva, Switzerland, 2001; pp 55–59
- (10) Zhang, M.; Jin, Z. S.; Zhang, J. W. *J. Mol. Catal. A: Chem.* **2005**, *225*, 59–63.
- (11) Li, Q. Y.; Wang, K.; Zhang, S. L.; Zhang, M. *J. Mol. Catal. A: Chem.* **2006**, *258*, 83–88.
- (12) Vorontsov, A. V.; Savinov, E. N.; Jin, Z. S. *J. Photochem. Photobiol. A: Chem.* **1999**, *125*, 113–117.
- (13) Hwang, S.; Lee, M. C.; Choi, W. *Appl. Catal., B* **2003**, *46*, 49–63.
- (14) Obee, T. N.; Brown, R. T. *Environ. Sci. Technol.* **1995**, *29*, 1223–1231.
- (15) Kim, J. H.; Zhu, K.; Yan, Y. F. *Nano Lett.* **2010**, *10*, 4099–4104.
- (16) Pichat, P.; Disdier, J. *Catal. Today.* **2000**, *63*, 363–369.
- (17) Ao, C. H.; Lee, S. C. *Appl. Catal., B* **2003**, *42*, 119–129.
- (18) Yan, H.; Yang, H. *J. Alloys Compd.* **2011**, *509*, 26–29.
- (19) Bandara, J.; Udawatta, C. P. K.; Rajapakse, C. S. K. *Photochem. Photobiol. Sci.* **2005**, *4*, 857–861.
- (20) Xiang, Q.; Yu, J.; Jaroniec, M. *J. Am. Chem. Soc.* **2012**, *134*, 6575–6578.
- (21) Yu, J.; Qi, L.; Jaroniec, M. *J. Phys. Chem. C* **2010**, *114*, 13118–13125.
- (22) Ma, T. Y.; Cao, J. L.; Shao, G. S. *J. Phys. Chem. C* **2009**, *113*, 16658–16667.
- (23) Amama, P. B.; Itoh, K.; Murabayashi, M. *J. Mater. Sci.* **2004**, *39*, 4349–4351.
- (24) Meekins, B. H.; Kamat, P. V. *J. Phys. Chem. Lett.* **2011**, *2*, 2304–2310.
- (25) López, D.; Gómez-Segura, J. *J. Catal.* **2008**, *255*, 29–39.
- (26) Crihan, D.; Knapp, M.; Zweidinger, S. *Angew. Chem.* **2008**, *120*, 2161–2164.
- (27) Studt, F.; Abild-Pedersen, F.; Hansen, H. A. *ChemCatChem.* **2010**, *2*, 98–102.
- (28) Hofmann, J. P.; Zweidinger, S.; Knapp, M. *J. Phys. Chem. C* **2010**, *114*, 10901–10909.
- (29) Over, H. *Chem. Rev.* **2012**, *112*, 3356–3426.
- (30) Xiang, G.; Shi, X. J.; Wu, Y. L. *Sci. Rep.* **2012**, *2*, 1–6.
- (31) Seki, K. *Catal. Surv. Asia* **2010**, *14*, 168–175.
- (32) Bamwenda, G. R.; Tsubota, S. *Catal. Lett.* **1997**, *44*, 83–87.
- (33) Ismail, A. A.; Bahnemann, D. W.; Al-Sayari, S. A. *Appl. Catal., A* **2012**, *431–432*, 62–68.
- (34) Guo, X.; Guo, D. J.; Qiu, X. P. *J. Power Sources* **2009**, *194*, 281–285.
- (35) Lee, J.; Park, H.; Choi, W. *Environ. Sci. Technol.* **2002**, *36*, 5462–5468.
- (36) Weiher, N.; Beesley, A. M.; Tsapatsaris, N. *J. Am. Chem. Soc.* **2007**, *129*, 2240–2241.
- (37) Kalyanasundaram, K.; Borgarello, E.; Gratzel, M. *Helv. Chim. Acta* **1981**, *64*, 362–366.
- (38) Duonghong, D.; Borgarello, E.; Gratzel, M. *J. Am. Chem. Soc.* **1981**, *103*, 4685–4690.
- (39) Borgarello, E.; Kiwi, J.; Pelizzetti, E.; Visca, M.; Gratzel, M. *J. Am. Chem. Soc.* **1981**, *103*, 6324–6329.
- (40) Borgarello, E.; Kiwi, J.; Pelizzetti, E.; Visca, M.; Gratzel, M. *Nature* **1981**, *289*, 158–160.
- (41) Kalyanasundaram, K.; Gratzel, M. *Angew. Chem., Int. Ed. Engl.* **1979**, *18*, 701–702.
- (42) Lin, F.; Zhang, Y. N.; Li, C. *Appl. Catal., B* **2012**, *127*, 363–370.
- (43) Kawai, T.; Sakata, T. *Chem. Phys. Lett.* **1980**, *72*, 87–89.
- (44) Over, H.; Seitsonen, A. P.; Lundgren, E. *Chem. Phys. Lett.* **2001**, *342*, 467–472.
- (45) Triggs, P. *Helv. Phys. Acta* **1985**, *58*, 657–714.
- (46) Cromer, D. T.; Herrington, K. *J. Am. Chem. Soc.* **1955**, *77*, 4708–4709.
- (47) Czekaj, I.; Piazzesi, G.; Wokaun, A. *Surf. Sci.* **2006**, *600*, 5158–5167.
- (48) D'Arienzo, M.; Carbajo, J.; Bahamonde, A.; Crippa, M.; Polizzi, S.; Scotti, R.; Wahba, L.; Morazzoni, F. *J. Am. Chem. Soc.* **2011**, *133*, 17652–17661.

- (49) Zhao, Y.; Ma, W.; Li, Y.; Ji, H.; Chen, C.; Zhu, H.; Zhao, J. *Angew. Chem.* **2012**, *124*, 3242–3246.
- (50) Liu, M.; Piao, L.; Zhao, L.; Ju, S.; Yan, Z.; He, T.; Zhou, C.; Wang, W. *Chem. Commun.* **2010**, *46*, 1664–1666.
- (51) Seitsonen, A. P.; Over, H. *Surf. Sci.* **2009**, *603*, 1717–1723.
- (52) Wendt, S.; Seitsonen, A. P.; Kim, Y. D. *Surf. Sci.* **2002**, *505*, 137–152.
- (53) Madhavaram, H.; Idriss, H.; Wendt, S. *J. Catal.* **2001**, *202*, 296–307.